Volume 12
Number 5
7 February 2021
Pages 1571–1946

# Chemical Science

rsc.li/chemical-science

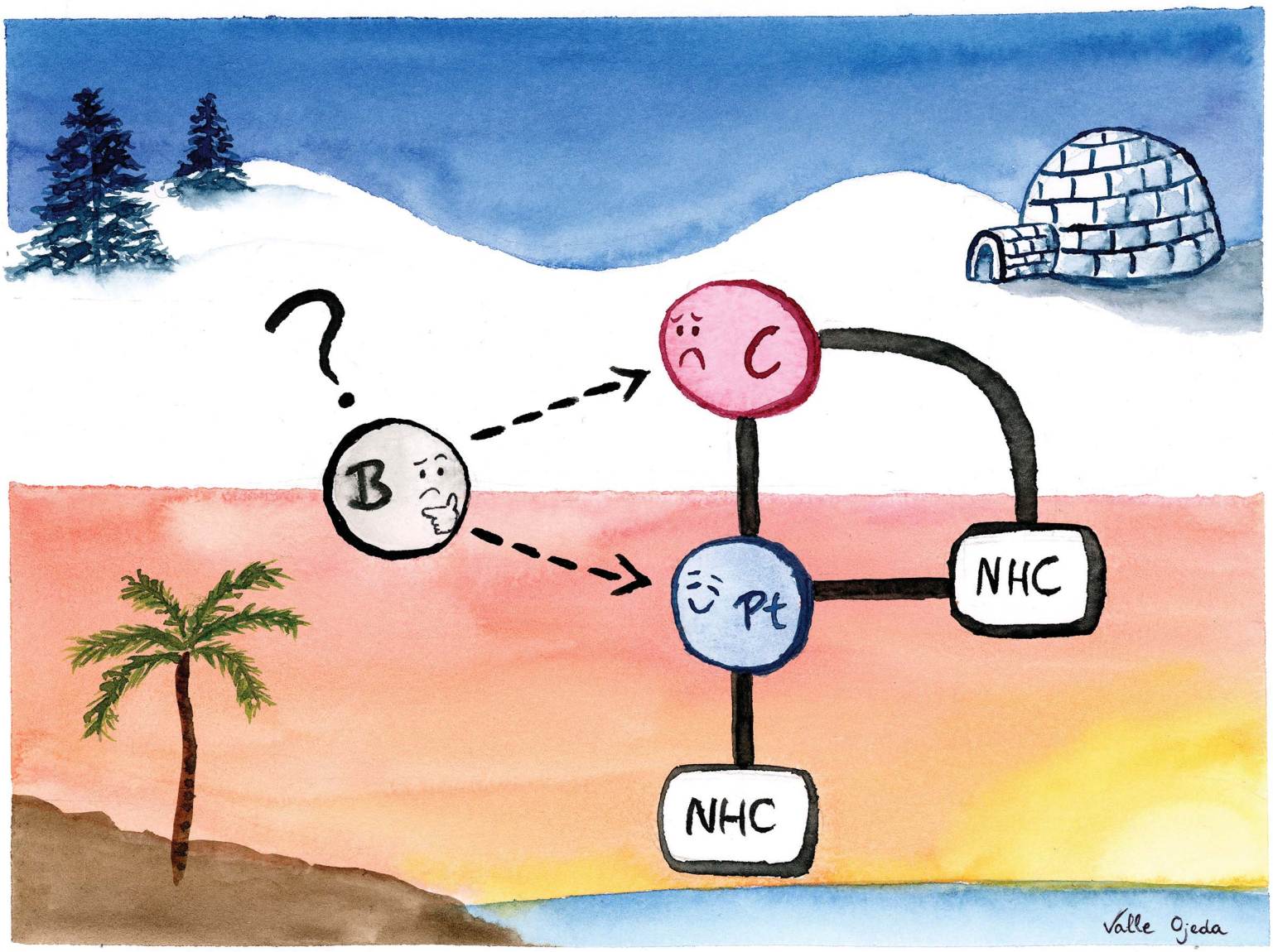


ISSN 2041-6539

ROYAL SOCIETY OF CHEMISTRY

**EDGE ARTICLE**

Agustí Lledós, Salvador Conejero *et al.*
Reversible carbon–boron bond formation at platinum centers through σ-BH complexes

Chemical Science

ROYAL SOCIETY OF CHEMISTRY

EDGE ARTICLE

View Article Online
View Journal | View Issue



Cite this: *Chem. Sci.*, 2021, **12**, 1647

All publication charges for this article have been paid for by the Royal Society of Chemistry

# Reversible carbon–boron bond formation at platinum centers through σ-BH complexes†

Pablo Ríos, [a] Rocío Martín-de la Calle,[a] Pietro Vidossich,[b] Francisco José Fernández-de-Córdova,[a] Agustí Lledós*[c] and Salvador Conejero *[a]

Received 6th October 2020
Accepted 9th November 2020

DOI: 10.1039/d0sc05522k

rsc.li/chemical-science

A reversible carbon–boron bond formation has been observed in the reaction of the coordinatively unsaturated, cyclometalated, Pt(II) complex [Pt(I$^t$Bu$^i$Pr′)(I$^t$Bu$^i$Pr)][BAr$^F$], **1**, with tricoordinated boranes $HBR_2$. X-ray diffraction studies provided structural snapshots of the sequence of reactions involved in the process. At low temperature, we observed the initial formation of the unprecedented σ-BH complexes [Pt($HBR_2$)(I$^t$Bu$^i$Pr′)(I$^t$Bu$^i$Pr)][BAr$^F$], one of which has been isolated. From −15 to +10 °C, the σ-BH species undergo a carbon–boron coupling process leading to the platinum hydride derivative [Pt(H)(I$^t$Bu$^i$Pr–$BR_2$)(I$^t$Bu$^i$Pr)][BAr$^F$], **4**. Surprisingly, these compounds are thermally unstable undergoing carbon–boron bond cleavage at room temperature that results in the 14-electron Pt(II) boryl species [Pt($BR_2$)(I$^t$Bu$^i$Pr)$_2$][BAr$^F$], **2**. This unusual reaction process has been corroborated by computational methods, which indicate that the carbon–boron coupling products **4** are formed under kinetic control whereas the platinum boryl species **2**, arising from competitive C–H bond coupling, are thermodynamically more stable. These findings provide valuable information about the factors governing productive carbon–boron coupling reactions at transition metal centers.

## 1. Introduction

The formation of C–B bonds, mediated by transition metal complexes, has become an important tool for the synthesis of organoboron compounds,[1] an important family of organic molecules in synthetic organic chemistry and in materials science.[2] From the mechanistic point of view, there have been several reports that point to the participation of σ-BH (σ-borane) complexes as key intermediates in the formation of the carbon–boron bonds in metal-alkyl or -aryl compounds. For example, Hartwig *et al.* have shown, by means of DFT calculations, that σ-BH complexes of rhodium and tungsten are transient species in the borylation of alkanes, where the driving force is the formation of the C–B bonds (Scheme 1).[3]

Although most of this type of C–H borylation processes have been carried out using rhodium and iridium systems,[4] there have been a few reports on the utilization of platinum complexes for the formation of C–B bonds, either in stoichiometric reactions or in catalytic processes.[5] Turculet and Stradiotto reported the dehydrogenative coupling of B–H/C–H bonds at a Pt(II) center,[5a] whereas Chatani, Tobisu *et al.* suggested the participation of σ-BH complexes in the platinum-catalyzed borylation of arenes.[5b,c] However, the interaction of tricoordinated hydroboranes with platinum centers leading to σ-BH complexes has proven elusive.[6] In addition, examples of transition metal σ-borane alkyl complexes [M(R)($HBR_2$)] are extremely rare, and those that have been isolated did not show further reactivity involving the formation of carbon–boron bonds.[7] Isolation of this type of compounds might offer an invaluable opportunity for determining the factors that can lead

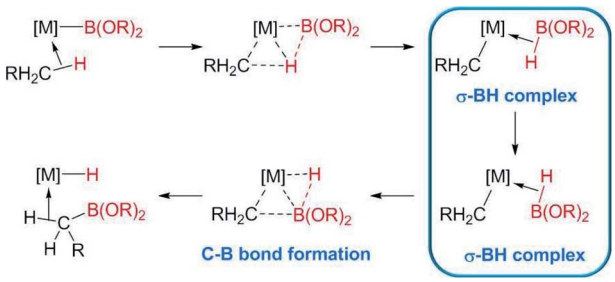


Scheme 1 σ-BH complexes proposed as intermediates in the borylation of C–H bonds of alkanes reported by Hartwig *et al.*[3]

[a]*Instituto de Investigaciones Químicas (IIQ), Departamento de Química Inorgánica, CSIC and Universidad de Sevilla, Centro de Innovación en Química Avanzada (ORFEO-CINQA), C/ Américo Vespucio 49, Sevilla, 41092, Spain. E-mail: sconejero@iiq.csic.es*

[b]*Molecular Modeling & Drug Discovery Laboratory, Istituto Italiano di Tecnologia, Via Morego 30, 16163 Genoa, Italy*

[c]*Departament de Química, Universitat Autònoma de Barcelona, Edifici Cn, Cerdanyola del Vallès, 08193, Spain. E-mail: agusti@klingon.uab.es*

† Electronic supplementary information (ESI) available: Experimental details, spectroscopic, computational data (PDF). X-ray crystallographic data (CIF). Cartesian coordinates of the selected DFT optimized structures (*XYZ*). CCDC 2033931–2033934. For ESI and crystallographic data in CIF or other electronic format see DOI: 10.1039/d0sc05522k

to competitive carbon–boron or carbon–hydrogen coupling products.

In this article, we report the spectroscopic observation and isolation of platinum σ-BH complexes that undergo either a carbon–boron coupling process or formation of platinum-boryl complexes as a function of temperature. The whole sequence of events underlying these processes has been followed by NMR and X-ray diffraction studies and investigated by DFT calculations.

## 2. Results and discussion

### 2.1 Synthesis of Pt(II) boryl complexes

In previous studies we have reported that some low-coordinate cationic platinum(II) complexes can interact with tetra-coordinated boranes, L·$BH_3$ (L = pyridine, amine), leading to stable adducts or to catalytic boron–nitrogen coupling products (amine–borane dehydrocoupling).[8] In this context we have examined the reactivity of these platinum systems with tri-coordinated boranes derived from dioxa- and diaza-boroles. We have chosen cationic platinum(II) complex [Pt($I^{t}Bu^{i}Pr'$)($I^{t}Bu^{i}Pr$)][$BAr^{F}$], **1**, as starting material (where $I^{t}Bu^{i}Pr$ is 1-*tert*-butyl-3-isopropylimidazol-2-ylidene, and $I^{t}Bu^{i}Pr'$ its cyclometalated form through the *tert*-butyl substituent), since this system has been successfully used for the isolation of related σ-SiH derivatives.[9] When complex **1** was treated with either pinacol- (HBpin, **a**) or catechol–borane (HBcat, **b**), or 1,3,2-benzodiazaborolane (HBdab, **c**) in $CH_2Cl_2$ at 25 °C, boryl complexes **2a–c** were formed quantitatively according to NMR spectroscopy (Scheme 2). The reaction proceeds smoothly but reaction times vary considerably from dioxaboroles to the diazaborole, from 10 min to 15 h. The $^{1}H$ NMR spectra of these species reveal a highly symmetric environment of the NHC ligands, indicating their chemical equivalence.

The $^{11}B\{^{1}H\}$ NMR spectra exhibit two sets of signals, one for the Pt–B fragment and the other for the $BAr^{F}$ anion. The former resonate at $\delta$ 12.7, 14.7 and 8.8 for **2a–c**, respectively, showing coupling to $^{195}Pt$ in the range 1390–1700 Hz (see ESI†). Crystals of **2c** suitable for X-ray diffraction studies were grown by slow diffusion of $CH_2Cl_2$ solutions into pentane. Fig. 1 shows an ORTEP-type view of the cation. The platinum atom is surrounded by only three ligands, with a formal vacant site *trans* to the boryl moiety. Very weak, at best, agostic interactions are present in the molecule (the closest C to Pt is 3.1 Å away).[10] The Pt–B distance of 1.988(6) Å is similar to that reported by Braunschweig in related systems of the type *trans*-[$(Cy_3P)_2$Pt{B(X)X′}].[11]

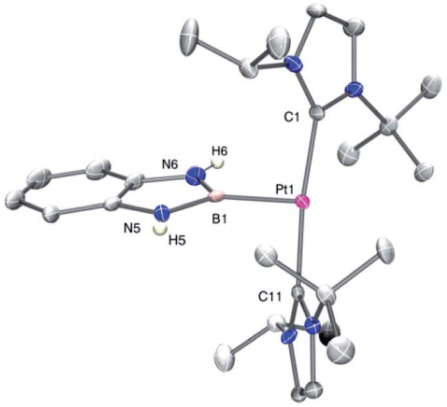


Fig. 1 ORTEP representation of the cation of complex **2c**. Hydrogen atoms (except those of the NH moieties) have been omitted for clarity. Selected bond distances (Å) and angles (°): Pt1–B1, 1.988(6); Pt1–C1, 2.015(5); Pt1–C11, 2.016(5); B1–N6, 1.424(7); B1–N5, 1.433(7); C1–Pt1–C11, 173.5(2); B1–Pt1–C1, 92.9(2); B1–Pt1–C11, 93.6(2).

### 2.2 Low-temperature reactivity studies: characterization and isolation of σ-BH Pt(II) complexes

In order to look for intermediates in the reaction process, and in particular to detect σ-BH complexes, low temperature NMR experiments have been carried out. The reaction of **1** with a slight excess of pinacolborane in an NMR tube in $CD_2Cl_2$ at −30 °C led to a clean reaction with formation of a new species that, according to multinuclear NMR, is the σ-BH complex **3a** (Scheme 3). The $^{1}H$ NMR is characterized by a broad signal in the hydride region at −3.93 ppm, showing coupling to $^{195}Pt$ ($^{1}J_{H,Pt}$ = 357 Hz). This signal becomes narrower upon $^{11}B$ decoupling (see Fig. S11 in the ESI†) and it has been assigned to the bridging Pt–H–B proton. The $^{11}B\{^{1}H\}$ spectrum shows, besides the signal for the $BAr^{F}$ anion and some excess of HBpin, a very broad signal at 21.8 ppm.[12] A similar behavior has been observed in the reaction of **1** with HBcat leading to **3b** ($^{1}H$ NMR: −3.28 ppm, $^{1}J_{H,Pt}$ = 327 Hz; $^{11}B\{^{1}H\}$ NMR: 21.3 ppm) and with HBdab producing **3c** ($^{1}H$ NMR: −2.32 ppm, $^{1}J_{H,Pt}$ = 339 Hz; $^{11}B$

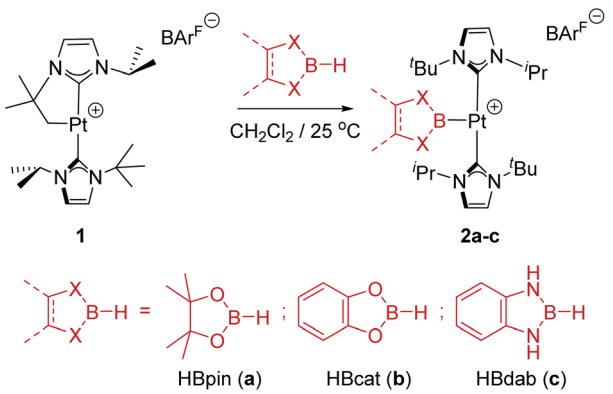


Scheme 2 Reaction of complex **1** with hydroboranes.

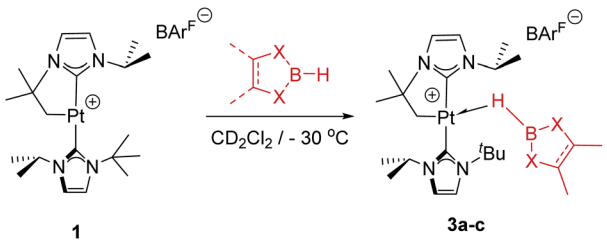


Scheme 3 Formation of σ-BH complexes **3a–c** at low T.

{$^1$H} NMR: 18.6 ppm). All these sigma complexes are stable at temperatures ranging from −15 to +10 °C, with complex **3c** being the most stable. In line with these findings, DFT calculations estimate favorable $\Delta G$ of formation at −30 °C of −2.3, −0.6 and −3.1 kcal mol$^{-1}$ for **3a**, **3b** and **3c**, respectively (see Fig. S33 in the ESI†).

The increased thermal stability of complex **3c** has allowed us to obtain crystals suitable for X-ray diffraction analysis by slow diffusion of $CH_2Cl_2$ solution into pentane at −25 °C (Fig. 2). The platinum center is found in a nearly planar environment, with two NHCs and one –$CH_2$– unit occupying three coordination sites and the B–H moiety the fourth. The angle defined by atoms C13–Pt1–H1 and Pt1–H1–B1 are 168.5(1)° and 105(2)°, respectively, very close to those observed in the related σ-SiH derivative [Pt(HSiEt$_3$)(I$^t$Bu$^i$Pr′)(I$^t$Bu$^i$Pr)][BAr$^F$] (173.1(1)° and 103(2)°).[9] The Pt1–H1 and H1–B1 bond distances are 1.69(4) Å and 1.19(3) Å, respectively. The latter is slightly elongated with respect to the B–H bond of boranes[13] and comparable to related σ-BH primary aminoborane complexes.[14] The Pt1···B1 distance of 2.31 Å is considerably larger than the sum of covalent radii (2.2 Å), suggesting that, if any, the interaction between these two atoms is weak.[15] In fact, topological analysis of the electron density and its laplacian (see ESI†) revealed the presence of bond critical points (BCPs) between Pt and H, and H and B, yet no BCP between Pt and B was observed.[16] This fact suggests that the coordination mode is better described as $\eta^1$-BH instead of the common $\eta^2$-BH mode reported for other transition metals.[6,13,17] Bonding interactions were further analyzed in terms of localized orbitals.[18] The centroid of the localized orbital corresponding to the B–H bond ($X_{BH}$, Fig. 3) is close to the H center, in agreement with a marked hydride character of this H atom, and is displaced from the B–H axis towards Pt, indicative of a perturbed sigma bond. At the same time, one Pt centroid ($X_{Pt}$) is slightly moved away (0.431 Å) from the nucleus, compared to the other Pt centroids (0.345–0.398 Å), and pointing to B. We have previously characterized similar interactions in cationic Pt(II) σ-silane complexes, which adopt a rare $\eta^1$-SiH coordination mode.[9]

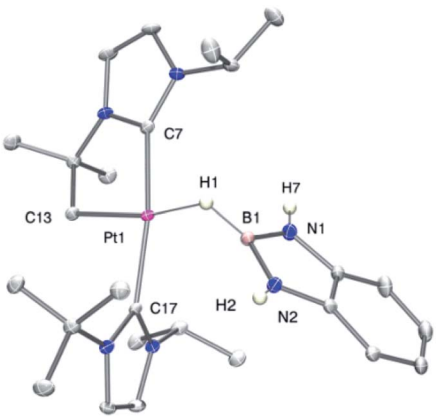


Fig. 2 Molecular structure of the cationic component as determined by X-ray diffraction of complex **3c** (ellipsoids at 30% probability). Selected bond distances (Å) and angles (°): Pt1–H1, 1.69(4); H1–B1, 1.19(3), Pt1–C13, 2.054(2); Pt1–H1–B1, 105(2); C13–Pt1–H1, 168.5(1).

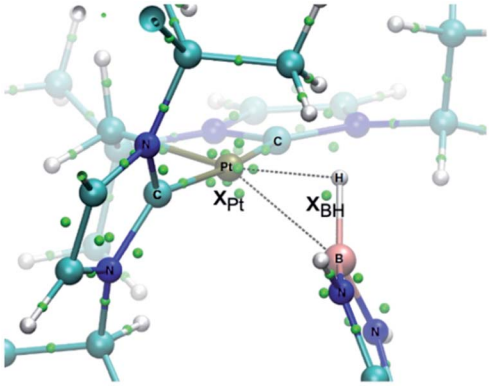


Fig. 3 Localized orbital analysis of **3c**. The molecular structure is overlaid with the centroids of the localized orbitals (small green dots). Dotted lines highlight the Pt–B and Pt–H distances.

As in the previously characterized $\eta^1$-SiH platinum complexes,[9] the coordination of the σ-bonded ligand is very flexible. We computed the energetic cost of deforming the Pt–H–B angle in **3c** (see Table S4 and Fig. S40†). Starting from the energy minimum at 101.6°, closing the angle to 78° or opening it to 154° requires less than 6 kcal mol$^{-1}$. More acute angles (68°) lead to borane dissociation instead of B–H bond cleavage, which contrasts with what was observed between **1** and hydrosilanes, for which closing the Pt–H–Si angle led ultimately to the Si–H oxidative addition.[9] Importantly, QTAIM analysis did not reveal any BCP between Pt and B in structures with acute Pt–H–B angles (Fig. S38 and S39†).

### 2.3 Thermal evolution of σ-BH Pt(II) complexes: reversible C–B coupling en route to boryl complexes

As mentioned before complexes **3a–c** are only marginally thermally stable, and upon warming at temperatures above −15 °C (**3a**), 0 °C (**3b**) or +10 °C (**3c**) undergo a rearrangement that involves the cleavage of the B–H bond and the formation of a new C–B bond leading to complexes **4a–c** (Scheme 4). The reaction is particularly clean in the case of complex **3a**, for

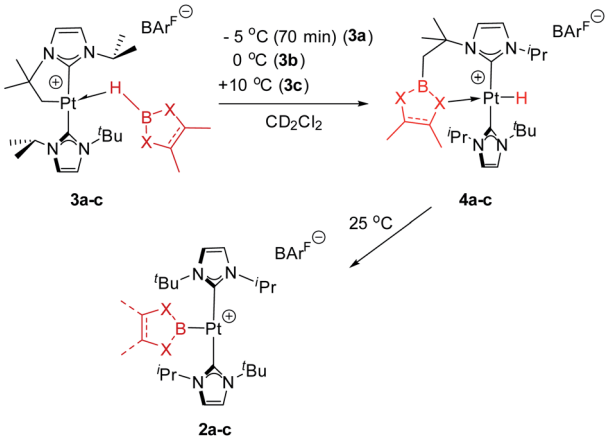


Scheme 4 Rearrangement of complexes **3a–c**.

which a progressive formation of **4a** is observed before it undergoes further rearrangement (see below). When complex **3a** is allowed to stand at −5 °C for *ca.* 70 min it undergoes B–H bond cleavage of the borane leading to hydride species **4a**, arising from a C–B coupling process with the Pt–$CH_2$ unit. In the $^1$H NMR spectrum the signal of the BH proton of complex **3a** progressively disappears, whereas a new narrow signal in the hydride region at −27.11 ppm simultaneously appears, showing a large coupling constant to $^{195}$Pt of 2167 Hz. This value is smaller than that observed for complex [Pt(H)($I^tBu^iPr$)$_2$][$BAr^F$] ($^1J_{H,Pt}$ = 2496 Hz).[19] In addition, the diastereotopic Pt–$CH_2$ protons in **3a** merge into a singlet resonance at 2.44 ppm in **4a**,[20] that correlates in the $^1$H, $^{13}$C-HSQC spectrum with a very broad resonance at 26.8 ppm. The $^{11}$B{$^1$H} NMR spectrum shows a very broad signal at 32.9 ppm. All these data support the platinum-hydride structure shown in Scheme 4, but definite evidence came from X-ray diffraction studies of complex **4a** obtained at −20 °C. Fig. 4 shows the cationic fragment of complex **4a**. The hydride ligand has been localized in the difference Fourier map. The structure confirms the formation of a C–B bond, as anticipated by NMR analysis. Moreover, one of the oxygen atoms of the pinacol moiety is interacting with the platinum center (Pt–O bond distance, 2.247(3) Å), *trans* to the hydride ligand, which explains the reduction of the $^1J_{H,Pt}$ coupling constant of the hydride compared to that in [Pt(H)($I^tBu^iPr$)$_2$][$BAr^F$].[19,21]

With respect to complexes **3b** and **3c**, a similar rearrangement is observed, although in a different range of temperatures. However, as the temperature increases, mixtures of these compounds together with intermediates **4b**, **c** and the final boryl complexes **2b**, **c** coexist, hampering full characterization of intermediates **4b**, **c** (see Fig. S25–S28 in the ESI†). Despite this, the signals observed in the hydride region of the $^1$H NMR spectra are consistent with formation of these transient species (**4b**: −24.7 ppm, $^1J_{H,Pt}$ = 2459 Hz at 5 °C; **4c**: −21.06; $^1J_{H,Pt}$ = 1905 Hz at 20 °C), as those in the $^{11}$B{$^1$H} NMR (**4b**: 33.4 ppm; **4c**: 29.6 ppm). It's worth noting the variations in the magnitude of the $^1J_{H,Pt}$ coupling constants of these Pt–H hydrides. In **4b** the value of 2459 Hz is higher than that of complex **4a**, and close to the hydride derivative [Pt(H)($I^tBu^iPr$)$_2$] [$BAr^F$], whereas a smaller value of 1906 Hz is observed in **4c**. Since the $^1J_{H,Pt}$ values are sensitive to the presence and nature of ligands *trans* to the hydride, the interaction of the oxygen atom with the platinum center in **4b** is weaker than in **4a** whereas, expectedly, the nitrogen atom has a stronger interaction with the platinum atom in **4c**.[21] This has important implications in the subsequent reactivity. All complexes **4** evolve at 25 °C into boryl species **2**, but the time required is slightly different between **4a** and **4b**, and markedly different for **4c**. The fastest is **4b**, requiring 10 min to be fully converted into **2b**, while **4a** rearrange in *ca.* 35 min. On the other hand, **4c** undergoes the C–B bond cleavage after 15 h. Thus, it appears that the stronger the interaction of the X (X = O, N) atom of the boryl fragment with the platinum center in complexes **4**, the longer it takes to transform **4** into the boryl species **2**. Therefore, we reasoned that de-coordination of the X atom to open a vacant site at the platinum center is required for the cleavage of the C–B bond leading to the boryl species **2**. In order to prove this, intermediate **4a** was reacted at −5 °C with $^t$BuNC (Scheme 5), leading to the 16-electron Pt(II) complex **5**. This compound is very stable, and no cleavage of the C–B bond is observed at 25 °C in solution, therefore corroborating the need for the vacant site to promote the rearrangement of hydride complexes **4** into boryl species **2**.

### 2.4 Mechanistic analysis of C–B and C–H bond formation

The observed reactivity of the **1** + $HBR_2$ systems summarized in Scheme 4 suggests a sequential mechanism in which first C–B and Pt–H bonds are formed (compounds **4a–c**) and then cleaved[22] leading to C–H and Pt–B bonds (compounds **2a–c**). To unravel atomic and electronic rearrangements taking place in these systems, we carried out DFT calculations (M06 functional) in dichloromethane solvent (SMD continuum model) using species **1** and HBpin (**a**). Details of the calculations are given in the ESI.† Contrary to expectations, however, we found that it is not possible to directly interconvert **4a** into **2a**. All attempts made to find such a pathway resulted in high energy species (see

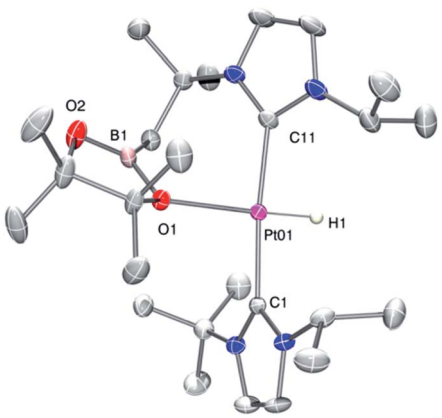


Fig. 4 Molecular structure of the cationic component as determined by X-ray diffraction of complex **4a** (ellipsoids at 30% probability).

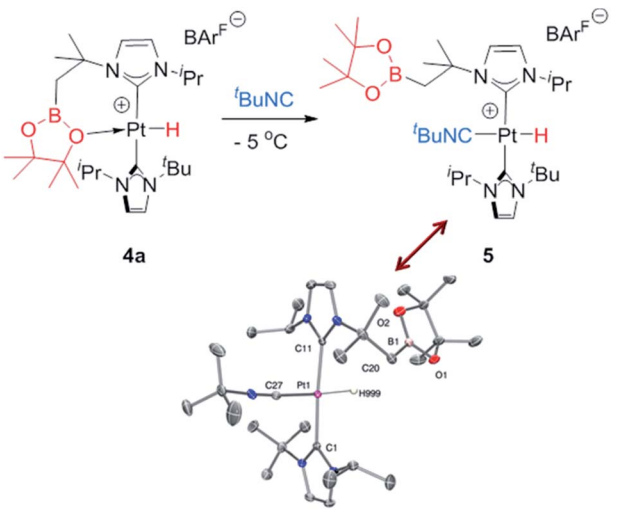


Scheme 5 Synthesis of complex **5** (top) and molecular structure of its cationic component (bottom).

High Energy Transition States section in ESI†). The solution to this issue came by recognizing the analogy with the borylation of alkanes (Scheme 1).[3] Considering the σ-BH complex (here **3a**) the system can evolve towards the formation of a C–B bond (complex **4a**) or with the formation of a C–H bond (complex **2a**). Moreover, when raising the temperature, **4a** transforms into **2a** (Scheme 6).

We started the exploration from σ-BH complex **3a**. However, with the *trans*-NHC arrangement in **3a**, all transition states for transferring a H atom to the cyclometalated methylene fragment and forging a Pt–B bond, yielding complex **2a** (C–H bond formation), or transferring the Bpin and forming a Pt–H bond, yielding **4a** (C–B bond formation), are high in energy (34.0 and 28.5 kcal mol$^{-1}$ above the reagents, respectively; see Fig. S48 and S49 in the ESI†) and inconsistent with the experimental observations. We thus searched for alternative routes.

$Pt(NHC)_2$ fragments, even with bulky NHC ligands, are known to be rather flexible around the C–Pt–C angle.[23] In previous works we have shown that *trans–cis* isomerizations of $Pt(NHC)_2$ fragments can occur in their reactions with $H_2$ [24] and silanes.[19] Thus, we investigated mechanisms containing species with a *cis* geometry of the NHC ligands. Starting from complex **1**, *trans–cis* isomerization requires overcoming a barrier of 12.8 kcal mol$^{-1}$ and yields species **1-*cis***, 11.1 kcal mol$^{-1}$ above the origin (see Fig. S50 in the ESI†) presumably due to the increased steric bulk between the isopropyl chain of the cyclometalated NHC ligand and the other NHC fragment. Coordination of HBpin to **1-*cis*** gives a σ-BH complex, for which we found two possible orientations of the HBpin ligand relative to the $Pt(NHC)_2$ fragment (**3a-*cis*** and **3a-*cis*′**, Fig. 5). Both display a $\eta^1$-BH coordination mode, with geometrical parameters of the Pt–H–B fragment resembling those of **3a**. In **3a-*cis*** (7.8 kcal mol$^{-1}$ above **1** + HBpin), the B atom is closer to the methylene unit than the H atom (C···B(H)pin = 2.84 Å *vs.* C···H(Bpin) = 3.05 Å) with a Pt–H–B angle of 100.5°. On the contrary, in **3a-*cis*′** (10.0 kcal mol$^{-1}$) HBpin places its H atom closer to the methylene unit than the Bpin fragment (C···H(Bpin) = 2.57 Å *vs.* C···B(H)pin = 3.54 Å) with a Pt–H–B angle of 109.2°.

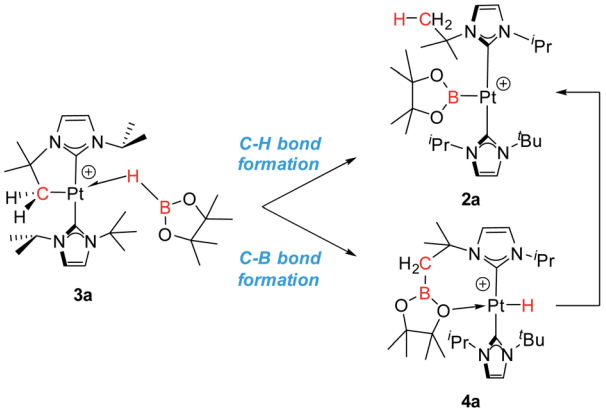


Scheme 6 Different reactivity pathways considered in DFT calculations.

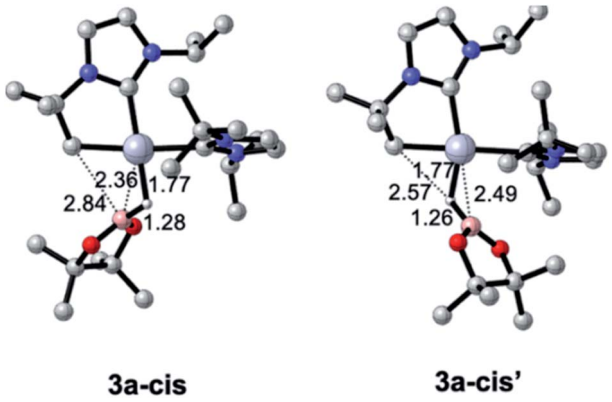


Fig. 5 Optimized geometries of σ-BH complexes with a *cis*-arrangement of NHC ligands.

The computed Gibbs energy profile assuming a *cis* arrangement of the NHC ligands is depicted in Fig. 6. **3a-*cis*** is the starting point of the C–B bond coupling pathway (Fig. 6, green trace). From this point, the B–H bond is cleaved through **TS1** (15.6 kcal mol$^{-1}$) in a process where the boryl group is transferred to the methylene fragment (C–B bond formation) at the same time that a Pt–H bond is created. The resulting hydride species **Int1** (7.5 kcal mol$^{-1}$) features an agostic interaction through one of the C–H bonds from the $CH_2$ group (H–Pt = 1.89 Å, C–H–Pt = 107.5°)[10] that stabilizes the vacant position of the complex. Further stabilization is observed when one of the oxygen groups from Bpin coordinates to platinum as in **4a-*cis***(2.0 kcal mol$^{-1}$), due to its higher electron donation ability. This exchange of ligands takes place through **TS2** (15.4 kcal mol$^{-1}$). Once **4a-*cis*** is formed, *cis* to *trans* isomerization through **TS3** (13.6 kcal mol$^{-1}$) yields experimentally observed complex **4a**, which exhibits both NHC ligands in a *trans* geometry. During isomerization, coordination of the Bpin fragment through oxygen is lost, giving species **Int2**, which consists of a cationic Pt(II) hydride complex analogous to $[Pt(H)(I^tBu_2)_2]^+$, previously calculated by our group (the main difference being the presence of Bpin in one of the carbene ligands and isopropyl instead of *tert*-butyl substituents).[25] Finally, coordination of one oxygen of the Bpin fragment to the metal yields the C–B coupling product **4a**, at −6.8 kcal mol$^{-1}$.

**3a-*cis*′** has the right orientation of the HBpin ligand to start C–H bond coupling pathway (Fig. 6, red trace). From here, the H atom is transferred to the C atom at the same time than the Pt–B bond is formed. This step takes place through **TS4** (22.1 kcal mol$^{-1}$), after which the corresponding boryl complex **Int3** is formed. Right after, isomerization *via* **TS5** (10.1 kcal mol$^{-1}$) gives the experimentally observed boryl derivative **2a**, which is the thermodynamically most stable compound of the whole energy profile.

From the Gibbs energy profile in Fig. 6 it can be inferred that, at low temperature, the product entailing crossing the lowest barrier will be formed (kinetic control). This is the hydride species **4a**, arising from a C–B coupling process with the Pt–$CH_2$ unit, which is formed from **3a-*cis*** after crossing a barrier of only

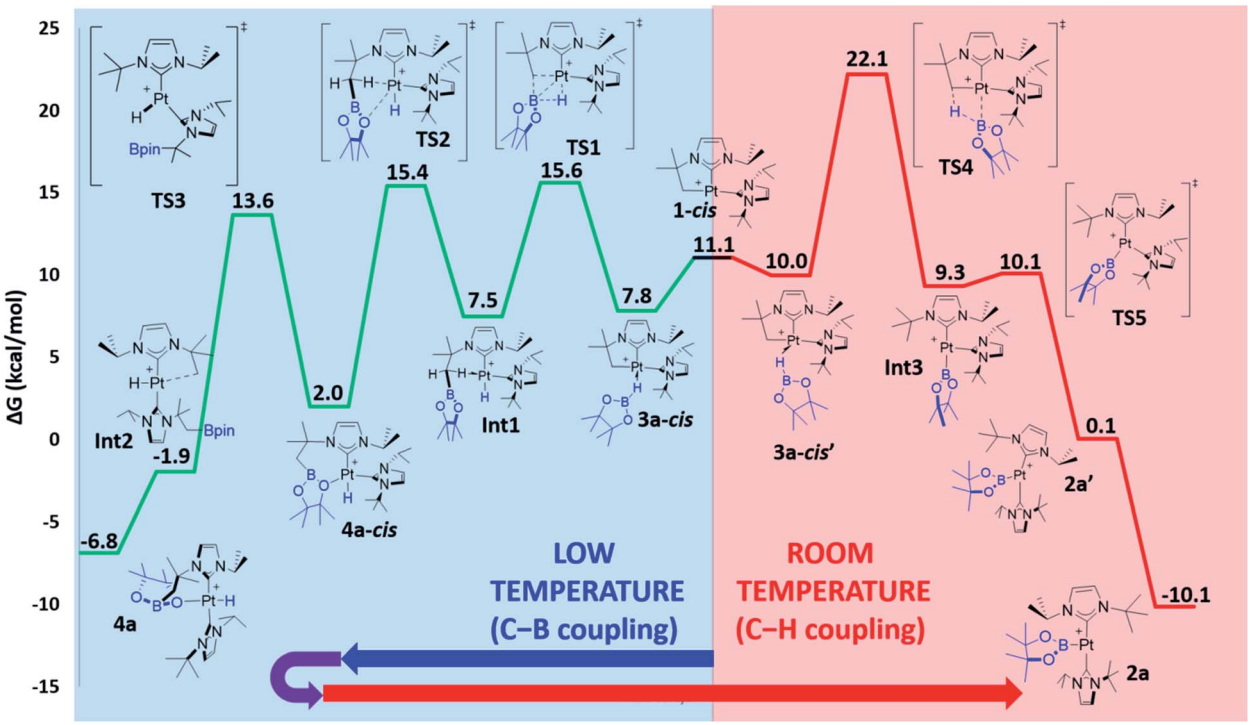


Fig. 6 Gibbs energy profile in dichloromethane for the C–B (green trace) and C–H (red trace) bond formation pathways (NHCs in *cis*) upon reaction between **1** and HBpin. Gibbs energies at 298 K in kcal mol$^{-1}$. The Gibbs energy of **1** + HBpin has been taken as zero-energy.

7.8 kcal mol$^{-1}$ (**TS1**). However, going back from **4a** to **3a-*cis*** requires an activation of only 22.4 kcal mol$^{-1}$, which can be provided raising enough the temperature. At 25 °C transition state **TS4** (22.1 kcal mol$^{-1}$) can be overcome and the reaction is driven by the formation of the most stable product, **2a** (thermodynamic control). The boryl complex **2a** is formed *via* a C–H coupling process. The rationalization for the experimental observations combines the C–B (Fig. 6, green trace) and C–H (Fig. 6, red trace) bond formation pathways: at low temperatures, C–B bond formation takes place through the aforementioned described mechanism, yielding **4a**. Then, increasing the temperature to 25 °C allows the system to undergo the reverse pathway, reaching **3a-*cis*** and, after a conformational change, **3a-*cis*′**, which initiates the C–H coupling pathway leading to the most stable product **2a**. The different energetic barriers observed from **3a-*cis*** and **3a-*cis*′** leading to C–B or C–H coupling, respectively, might have (at least in part) a steric origin. The orientation of the pinacol substituents in **3a-*cis*′** is likely inducing some steric repulsions with the spectator NHC ligand in *cis* to it, and this might account for the different Pt⋯B bond distances (0.13 Å) observed in both **3a-*cis*** and **3a-*cis*′**. Reducing the steric effects on the borane might reduce the energy differences. In fact, as stated before, in the reaction carried out with HBcat, complexes **4b** and **2b** coexist in a certain range of temperatures, suggesting that, in this case, formation of C–B and C–H bonds have very similar energetic barriers.

### 2.5 Electronic analysis of C–B and C–H coupling processes

Exploration of the potential energy surface of **1** + HBpin system has allowed disclosing the mechanism for the formation of C–B and C–H coupling products and their interconversion. Calculations have shown that rupture of B–H and $H_2C$–Pt bonds and formation of either C–B and Pt–H or C–H and Pt–B bonds entail similar energy requirements. To reveal these bonding rearrangements we applied a localized orbital approach, which turned highly useful to analyze other organometallic reactions.[18] In this approach Kohn–Sham molecular orbitals are transformed into maximally localized orbitals (LMOs) and the centroids of these LMOs are computed for selected structures along the reaction path. The movement of the LMOs centroids along the reaction describes the electronic rearrangements taking place in the bond-breaking and bond-forming processes. In this way an arrow-pushing description of the C–B and C–H coupling processes can be obtained from DFT calculations. Recently, we applied this approach to analyze C–Si bond coupling reactions.[19]

Fig. 7 shows the relevant LMOs together with their centroids in three representative structures of the key chemical step of each process. The corresponding arrow-pushing schemes are also depicted in Fig. 7. The same LMOs are involved in both processes, one describing the $H_2C$–Pt bond and another corresponding to the B–H bond. Similarly to **3c**, in the initial structures **3a-*cis*** and **3a-*cis*′** the centroid of the B–H bond is displaced and very close to the H center, pointing to the hydride character of this atom. In the formation of the C–H bond the centroid of the C–Pt bond moves from the C–Pt axis to the C–H axis, while the centroid of the B–H bond moves from the B–H axis to the B–Pt axis. This corresponds to a sigma-CAM type reaction,[26] in which, formally, a proton is being transferred to the methylene fragment and a boryl

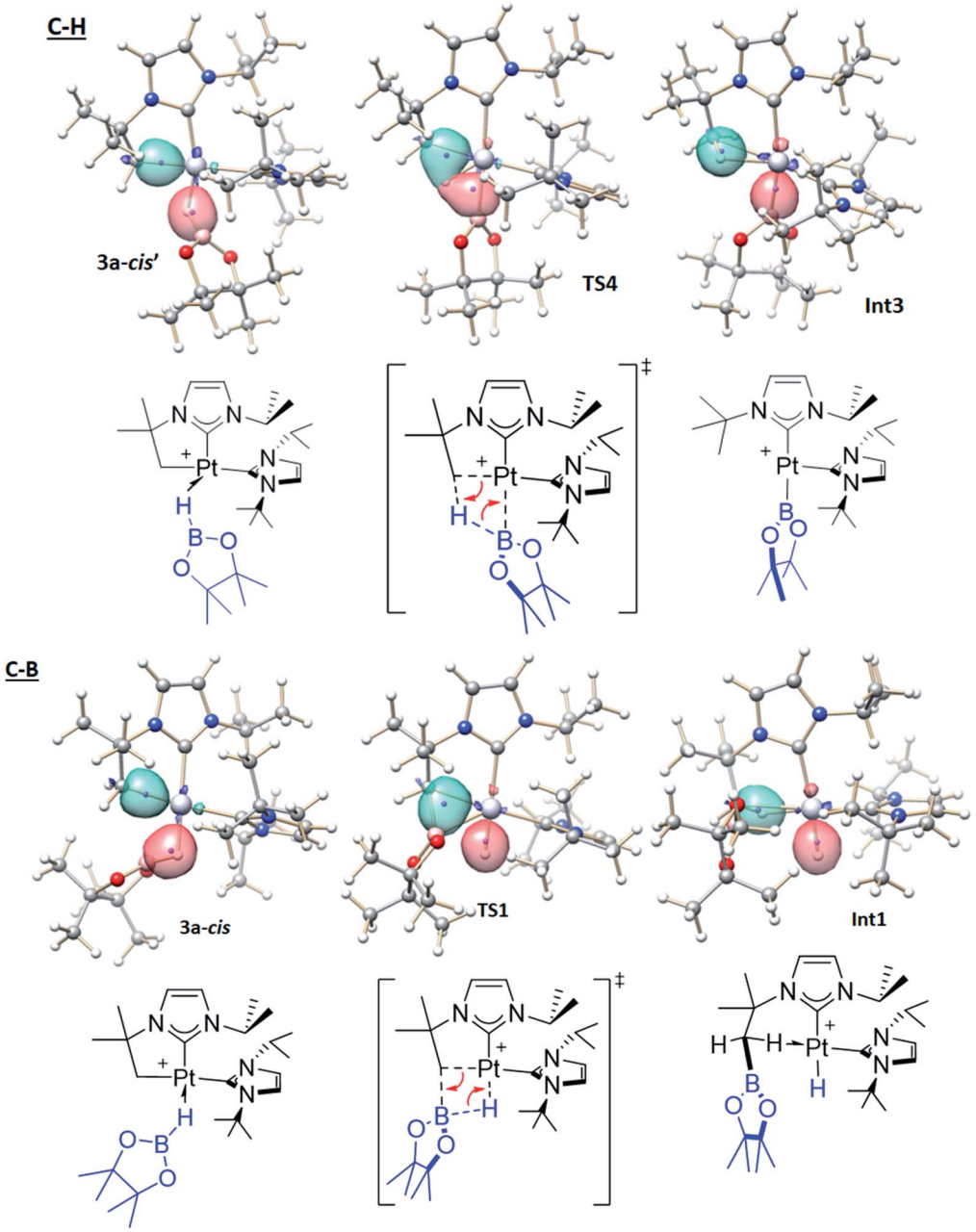


Fig. 7 C–H (top) and C–B (bottom) bond forming events from the analysis of the movements of the centroids of the localized orbitals, represented by small purple dots. Isosurfaces of the localized orbitals involved in the bond-breaking/bond-forming processes are also shown. For each process the deduced arrow-pushing scheme is also shown.

moiety is being formed. Conversely, in the formation of the C–B bond the centroid of the C–Pt bond moves from the C–Pt axis to the B–C axis, while the centroid of the B–H bond moves from the B–H axis to the H–Pt axis (again, a sigma-CAM rearrangement). Formally, a borinium[27] is being transferred to the methylene fragment and a metal-hydride is being formed. Therefore, the possibility to generate both boryl and borinium species from a platinum σ-BH complex is the underlying reason that allows both C–B and C–H bond coupling processes to take place in this system.

## 3. Conclusion

The low-electron count Pt(II) complex [Pt(I$^t$Bu$^i$Pr′)(I$^t$Bu$^i$Pr)][BAr$^F$], **1**, reacts with tri-coordinated boranes in a set of reactions that start with formation of σ-BH complexes, **3**, in which the interaction of the B–H fragment with the cationic platinum center adopts a rare $\eta^1$-BH coordination mode. These species evolve, as a function of temperature, by either formation of hydride complexes [Pt(H)(I$^t$Bu$^i$Pr′-BR$_2$)(I$^t$Bu$^i$Pr)][BAr$^F$], **4**, or platinum boryl derivatives [Pt(BR$_2$)(I$^t$Bu$^i$Pr)$_2$][BAr$^F$], **2**. We were able to detect species **3**, **4** and **2** by means of low temperature

NMR spectroscopy and, in some cases, by X-ray diffraction, providing snapshots of this unusual reactivity. DFT-based analyses support σ-complex assisted metathesis mechanisms (σ-CAM),[26] preceded by *trans* to *cis* isomerization of the NHC ligands. These calculations indicate that carbon-boron coupling products are energetically more accessible and that the competitive process leading to C–H bond coupling is more energy demanding. However, as the temperature increases, the thermodynamic stability of the final products determines the formation of the C–H bond coupling products. Steric effects between the substituents at the boryl fragment and the spectator NHC ligand in complexes **3a-*cis*** and **3a-*cis*′** might be behind the different energetic barriers. These results contribute to the mechanistic understanding of the factors that can lead to productive borylation and advance the design of new effective catalytic systems for such reactions.

## Conflicts of interest

There are no conflicts to declare.

## Acknowledgements

Financial support (FEDER contribution) from the MINECO (Projects CTQ2016-76267-P, CTQ2017-87889-P, PID2019-109312GB-I00 and RED2018-102387-T), the CSIC (AEPP_CTQ2016-76267-P) and the use of computational facilities of the Supercomputing Center of Galicia (CESGA) is gratefully acknowledged. P. R. thanks the Junta de Andalucía for a research grant.

## Notes and references

1 (*a*) J. V. Obligacion and P. J. Chirik, *Nat. Rev. Chem.*, 2018, **2**, 15–34; (*b*) M. Oestreich, E. Hartmann and M. Mewald, *Chem. Rev.*, 2013, **113**, 402–441; (*c*) I. Beletskaya and C. Moberg, *Chem. Rev.*, 2006, **106**, 2320–2354; (*d*) T. Ishiyamaa and N. Miyaura, *Chem. Rec.*, 2004, **3**, 271–280; (*e*) K. Burgess and M. J. Ohlmeyer, *Chem. Rev.*, 1991, **91**, 1179–1191; (*f*) T. B. Marder and N. C. Norman, *Topics in Catal*, ed. W. Leitner and D. G. Blackmond, Baltzer Science Publishers, Amsterdam, 1998, vol. 5, pp. 63–73.

2 (*a*) Synthesis and Applications of Organoboron Compounds, in *Topics in Organometallic Chemistry*, ed. E. Fernández and A. Whiting, Springer, Heidelberg, 2015; (*b*) *Boronic acids: preparation and applications in organic synthesis, medicine and materials*, ed. D. G. Hall, Wiley-VCH, Weinheim, 2nd edn, 2011, vol. 1 and 2.

3 (*a*) J. F. Hartwig, K. S. Cook, M. Hapke, C. D. Incarvito, Y. Fan, C. E. Webster and M. B. Hall, *J. Am. Chem. Soc.*, 2005, **127**, 2538–2552; (*b*) C. E. Webster, Y. Fan, M. B. Hall, D. Kunz and J. F. Hartwig, *J. Am. Chem. Soc.*, 2003, **125**, 858–859.

4 (*a*) A. Ros, R. Fernández and J. M. Lassaletta, *Chem. Soc. Rev.*, 2014, **43**, 3229–3243; (*b*) J. F. Hartwig, *Acc. Chem. Res.*, 2012, **45**, 864–872; (*c*) J. F. Hartwig, *Chem. Soc. Rev.*, 2011, **40**, 1992–2002; (*d*) I. A. I. Mkhalid, J. H. Barnard, T. B. Marder, J. M. Murphy and J. F. Hartwig, *Chem. Rev.*, 2010, **110**, 890–931; (*e*) T. Ishiyama and N. Miyaura, *J. Organomet. Chem.*, 2003, **680**, 3–11.

5 (*a*) C. M. Kelly, J. T. Fuller III, C. M. Macaulay, R. McDonald, M. J. Ferguson, S. M. Bischof, O. L. Sydora, D. H. Ess, M. Stradiotto and L. Turculet, *Angew. Chem., Int. Ed.*, 2017, **56**, 6312–6316; (*b*) T. Furukawa, M. Tobisu and N. Chatani, *Bull. Chem. Soc. Jpn.*, 2017, **90**, 332–342; (*c*) T. Furukawa, M. Tobisu and N. Chatani, *J. Am. Chem. Soc.*, 2015, **137**, 12211–12214.

6 (*a*) M. A. Esteruelas, A. M. López and M. Oliván, *Chem. Rev.*, 2016, **116**, 8770–8847; (*b*) I. M. Riddlestone, J. A. B. Abdalla and S. Aldridge, *Adv. Organomet. Chem.*, 2015, **63**, 1–38; (*c*) G. Alcaraz, M. Grellier and S. Sabo-Etienne, *Acc. Chem. Res.*, 2009, **42**, 1640–1649; (*d*) Z. Lin, Transition Metal σ-borane complexes, in *Contemporary metal boron chemistry I: borylenes, boryls, borane σ-complexes and borohydrides*, ed. T. B. Marder and Z. Lin, Springer, 2008, vol. 130, pp. 123–148.

7 (*a*) A. Cassen, Y. Gloaguen, L. Vendier, C. Duhayon, A. Poblador-Bahamonde, C. Raynaud, E. Clot, G. Alcaraz and S. Sabo-Etienne, *Angew. Chem., Int. Ed.*, 2014, **53**, 7569–7573; (*b*) C. Y. Tang, A. L. Thompson and S. Aldridge, *J. Am. Chem. Soc.*, 2010, **132**, 10578–10591.

8 (*a*) M. Roselló-Merino, R. J. Rama, J. Díez and S. Conejero, *Chem. Commun.*, 2016, **52**, 8389–8392; (*b*) M. Roselló-Merino, J. López-Serrano and S. Conejero, *J. Am. Chem. Soc.*, 2013, **135**, 10910–10913.

9 P. Ríos, H. Fouilloux, P. Vidossich, J. Díez, A. Lledós and S. Conejero, *Angew. Chem., Int. Ed.*, 2018, **57**, 3217–3221.

10 M. Brookhart, M. L. H. Green and G. Parkin, *Proc. Natl. Acad. Sci. U. S. A.*, 2007, **104**, 6908–6914.

11 (*a*) H. Braunschweig, K. Radacki and K. Uttinger, *Chem.–Eur. J.*, 2008, **14**, 7858–7866; (*b*) H. Braunschweig, P. Brenner, A. Müller, K. Radacki, D. Rais and K. Uttinger, *Chem.–Eur. J.*, 2007, **13**, 7171–7176; (*c*) H. Braunschweig, K. Radacki, D. Rais and D. Scheschkewitz, *Angew. Chem., Int. Ed.*, 2005, **44**, 5651–5654.

12 G. Alcaraz and S. Sabo-Etienne, *Coord. Chem. Rev.*, 2008, **252**, 2395–2409.

13 (*a*) J. C. Babón, M. A. Esteruelas, I. Fernández, A. M. López and E. Oñate, *Inorg. Chem.*, 2018, **57**, 4482–4491; (*b*) M. A. Esteruelas, I. Fernández, C. García-Yebra, J. Martín and E. Oñate, *Organometallics*, 2017, **36**, 2298–2307; (*c*) K. K. Pandey, *Inorg. Chem. Commun.*, 2008, **11**, 288–292.

14 (*a*) A. Kumar, N. A. Beattie, S. D. Pike, S. A. Macgregor and A. S. Weller, *Angew. Chem., Int. Ed.*, 2016, **55**, 6651–6656; (*b*) M. C. MacInnis, R. McDonald, M. J. Ferguson, S. Tobisch and L. Turculet, *J. Am. Chem. Soc.*, 2011, **133**, 13622–13633; (*c*) G. Alcaraz, L. Vendier, E. Clot and S. Sabo-Etienne, *Angew. Chem., Int. Ed.*, 2010, **49**, 918–920; (*d*) C. Y. Tang, A. L. Thompson and S. Aldridge, *Angew. Chem., Int. Ed.*, 2010, **49**, 921–925.

15 K. K. Pandey, *J. Mol. Struct.: THEOCHEM*, 2008, **855**, 18–26.

16 Different functionals and basis sets have been employed in these calculations, and no BCP between B and Pt has been observed in any case (see ESI† for more details).

17 (*a*) H. Braunschweig, K. Kraft, T. Kupfer and E. Siedler, *Z. Anorg. Allg. Chem.*, 2010, **636**, 2565–2567; (*b*) T. J. Hebden, M. C. Denney, V. Pons, P. M. B. Piccoli, T. F. Koetzle, A. J. Schultz, W. Kaminsky, K. I. Goldberg and D. M. Heinekey, *J. Am. Chem. Soc.*, 2008, **130**, 10812–10820; (*c*) M. G. Crestani, M. Muñoz-Hernández, A. Arévalo, A. Acosta-Ramírez and J. J. García, *J. Am. Chem. Soc.*, 2005, **127**, 18066–18073; (*d*) V. Montiel-Palma, M. Lumbierres, B. Donnadieu, S. Sabo-Etienne and B. Chaudret, *J. Am. Chem. Soc.*, 2002, **124**, 5624–5625; (*e*) S. Schlecht and J. F. Hartwig, *J. Am. Chem. Soc.*, 2000, **122**, 9435–9443; (*f*) J. F. Hartwig, C. N. Muhoro and X. He, *J. Am. Chem. Soc.*, 1996, **118**, 10936–10937.

18 G. Sciortino, A. Lledós and P. Vidossich, *Dalton Trans.*, 2019, **48**, 15740–15752.

19 P. Ríos, H. Fouilloux, J. Díez, P. Vidossich, A. Lledós and S. Conejero, *Chem.–Eur. J.*, 2019, **25**, 11346–11355.

20 Likely, a dynamic low energy barrier process (4.9 kcal $mol^{-1}$ from **4a** to **Int2**; see Figure 6) involving de-coordination/coordination of the O atom from platinum is responsible for the NMR equivalence of these $CH_2$ protons.

21 M. Ortuño, S. Conejero and A. Lledós, *Beilstein J. Org. Chem.*, 2013, **9**, 1352–1382.

22 For some examples of reversible C–B bond formation processes in organoboron compounds see: (*a*) Z.-C. He, S. K. Mellerup, L. Liu, X. Wang, C. Dao and S. Wang, *Angew. Chem., Int. Ed.*, 2019, **58**, 6683–6687; (*b*) S. K. Mellerup, C. Li, X. Wang and S. Wang, *J. Org. Chem.*, 2018, **83**, 11970–11977; (*c*) A. F. Eichhorn, S. Fuchs, M. Flock, T. B. Marder and U. Radius, *Angew. Chem., Int. Ed.*, 2017, **56**, 10209–10213; (*d*) B. E. Cowie and D. J. H. Emslie, *Organometallics*, 2015, **34**, 2737–2746; (*e*) D.-T. Yang, S. K. Mellerup, X. Wang, J.-S. Lu and S. Wang, *Angew. Chem., Int. Ed.*, 2015, **56**, 5498–5501.

23 G. C. Fortman, N. M. Scott, A. Linden, E. D. Stevens, R. Dorta and S. P. Nolan, *Chem. Commun.*, 2010, **46**, 1050–1052.

24 O. Rivada-Wheelaghan, M. Roselló-Merino, M. A. Ortuño, P. Vidossich, E. Gutiérrez-Puebla, A. Lledós and S. Conejero, *Inorg. Chem.*, 2014, **53**, 4257–4268.

25 M. A. Ortuño, P. Vidossich, S. Conejero and A. Lledós, *Angew. Chem., Int. Ed.*, 2014, **53**, 14158–14161.

26 R. N. Perutz and S. Sabo-Etienne, *Angew. Chem., Int. Ed.*, 2007, **46**, 2578–2592.

27 (*a*) D. Franz and S. Inoue, *Chem.–Eur. J.*, 2019, **25**, 2898–2926; (*b*) W. E. Piers, S. C. Bourke and K. D. Conroy, *Angew. Chem., Int. Ed.*, 2005, **44**, 5016–5036.